第 54 卷第 2 期
2026 年 2 月

硅 酸 盐 学 报
JOURNAL OF THE CHINESE CERAMIC SOCIETY

Vol. 54，No. 2
February，2026

http://jccsoc.cbpt.cnki.net

DOI：10.14062/j.issn.0454-5648.20250517

综 合 评 述

高温度梯度凝固成形超高温氧化物共晶陶瓷组织演变及力学性能研究进展

姜 浩，苏海军，余明辉，王若彤，申仲琳，郭一诺，张 卓，郭 敏

(西北工业大学，凝固技术全国重点实验室，西安 710072)

摘 要：为满足航空发动机等高端装备对超高温结构材料的严苛需求，基于熔体生长，兼具高熔点、优异抗氧化/耐腐蚀性能的氧化物共晶陶瓷已成为高温长时服役的关键候选材料。然而，如何突破氧化物共晶陶瓷大尺寸构件成形、凝固缺陷控制、强各向异性小平面共晶取向调控、以及强韧化等是推进该类材料工程化应用的关键。本文概述了提拉法、激光悬浮区熔、激光定向能量沉积及激光粉末床熔融 4 种制备超高温氧化物共晶陶瓷凝固成形技术的原理与发展现状，介绍了凝固过程中缺陷的形成机理和控制策略。重点阐述了氧化物共晶陶瓷的凝固组织演变规律与均细化调控方法、晶体取向选择影响因素和调控机制，以及氧化物共晶陶瓷的室温/高温力学性能与失效机理、高温组织稳定性及高温熔盐腐蚀性能研究进展。最后，展望了超高温氧化物共晶陶瓷在高梯度凝固成形、非平衡凝固缺陷抑制和多级协同强韧化 3 个方面的发展趋势。

关键词：氧化物共晶陶瓷；凝固成形；组织演变；性能调控
中图分类号：TQ174　　**文献标志码**：A　　**文章编号**：0454–5648(2026)02–0414–14
网络出版时间：2026–01–30



轻质高强的高温结构材料是支撑航空航天和国防安全领域的战略性材料，尤其作为高推重比航空发动机热端部件的核心材料，代表了材料科学与工程的前沿水平。发展具有优异综合性能的新型高温结构材料已成为各发达国家空天战略的迫切需求。当前，新一代推重比 10 以上航空发动机的涡轮进口温度已突破 1600 ℃，远超主流镍基单晶高温合金叶片约 1150 ℃的最高工作温度极限[1]。氮化硅(Si_3N_4)、碳化硅(SiC)和碳/碳(C/C)等先进超高温陶瓷基复合材料受限于其固有理化特性与现有烧结制备技术，在长期高温、富氧、水热腐蚀等极端服役环境中的抗氧化性、耐腐蚀性、高温组织稳定性及高温综合力学性能仍难以满足高推重比航空发动机发展的严苛需求[2]。因此，研发能在 1600 ℃以上极端环境中长期稳定工作的新型超高温结构材料及其先进制备技术，是提升航空发动机推重比、延长服役寿命、增强可靠性的重要保障，现已成为国际竞争的战略焦点。

超高温氧化物共晶陶瓷凭借高熔点、高强度及优异的抗氧化与耐腐蚀能力，被视为高温氧化环境中最具发展潜力的高温结构材料之一[3–6]。然而，使用传统粉末烧结技术制备的氧化物共晶陶瓷微观结构呈现典型多晶组织特征，晶界玻璃相和弱结合界面等结构缺陷严重削弱了氧化物共晶陶瓷的高温强度、组织稳定性及抗蠕变性能，导致氧化物共晶陶瓷在高温、富氧环境中所具备的优异抗氧化和耐腐蚀性能难以充分展现[7, 8]。近年来，基于液–固相变原理，采用定向凝固技术制备的氧化铝基共晶陶瓷在先进结构材料领域备受关注。该技术摒弃了传统陶瓷烧结思路，实现了熔体生长技术与氧化物共晶陶瓷优异性能的创新结合。例如，通过 Bridgman 法获得的熔体生长氧化铝/铝酸钆($GdAlO_3$, GAP)共

收稿日期：2025–06–30。　修订日期：2025–07–13。
基金项目：国家自然科学基金(52130204，52174376)；国家重点研发计划项目(2024YFB3714502)；陕西省重点研发计划项目(2024CY-GJHX-29，2024GX-ZDCYL-03-03)；宁波市科技计划项目(2025Z070)；西北工业大学凝固技术全国重点实验室开放课题(2025-TZ-01)。
第一作者：姜 浩(1996)，男，博士研究生。
通信作者：苏海军(1981)，男，博士，教授。

Received date: 2025–06–30.　**Revised date:** 2025–07–13.
First author: JIANG Hao (1996–), male, Doctoral candidate.
E-mail: jianghaonpu@mail.nwpu.edu.cn
Correspondent author: SU Haijun (1981–), male, Ph.D., Professor.
E-mail: shjnpu@nwpu.edu.cn

晶陶瓷的高温(1800 ℃)弯曲强度是相同共晶成分烧结陶瓷的 7 倍，在 1600 ℃的蠕变强度是同种烧结陶瓷的 13 倍[9, 10]；在 1700 ℃热暴露 1000 h 后，定向凝固制备的氧化铝/铝酸钇($Y_3Al_5O_{12}$，YAG)共晶陶瓷没有出现明显的微观组织粗化[11]。因此，基于熔体生长制备的氧化物共晶陶瓷有望成为在高温氧化环境中长期服役的新一代高温结构材料。

然而，氧化物共晶陶瓷的发展仍需克服诸多关键挑战。高熔点(>1600 ℃)多元复相氧化物共晶陶瓷在高温度梯度下的凝固特性及成形技术尚不完备，制约其工程化发展。受限于陶瓷本征脆性、熔体高黏度和低热导率，大尺寸复杂构件定向凝固过程易产生裂纹、气孔、缩孔、偏析等缺陷。同时，大部分氧化物单晶相呈现强各向异性的小平面生长特性。在高温度梯度下，晶体取向控制、共晶生长及形态转变极难控制。此外，面向航空发动机极端高温、氧化、腐蚀等恶劣服役环境，针对共晶陶瓷在极端条件下的高温性能等数据及机理研究仍较少。

针对以上问题，本文从氧化物共晶陶瓷的凝固成形技术与缺陷控制、凝固组织均细化与晶体取向调控、力学性能及失效机理 3 个方面重点阐述了本团队近年来在氧化物共晶陶瓷高梯度凝固成形与控形控性机理取得的研究进展，并展望了超高温氧化物共晶陶瓷未来的重点发展方向。

1　凝固成形技术与缺陷控制

得益于各国研究学者的持续探索，目前氧化物共晶陶瓷的凝固制备技术已呈现多元化发展，主要包括 Bridgman 法[12]、提拉法(CZ 法)[13]、边界外延生长法[14]、微抽拉法[15]、激光悬浮区熔(LFZM)[16]、水平定向凝固法(LPBF)[17]以及激光定向能量沉积(LDED)[18]和激光粉末床熔融(LDED)[19]等。表 1 对比了 4 种具有不同优势的凝固成形技术的温度梯度和常用工艺参数，并列出了其制备共晶陶瓷样件的宏观尺寸、微观组织尺度和力学性能。对应的氧化物共晶陶瓷的宏观样件和微观结构图片如图 1 所示。

1.1　CZ 法

CZ 法是一种重要的单晶生长技术，其成形原理如图 1 所示[30]。该方法将原材料置于铱(Ir)坩埚中熔化并均匀混合后，将籽晶下降并浸入熔体约 3~4 mm 深度进行引晶。在过冷度驱动下，熔体沿籽晶定向结晶。通过精确控制提拉速率、旋转速率及晶体直径等参数，获得特定尺寸的单晶晶体。

CZ 法的核心优势在于晶体悬垂于熔体中心生长，避免了与坩埚壁的直接接触，从而显著降低了生长过程中的应力；同时，该方法通过籽晶诱导能够实现对单晶晶体学取向的精确调控。然而，该方法也存在明显局限：籽晶的旋转运动与提拉杆的相互作用易诱发熔体对流，可能导致晶体结构扰动；此外，昂贵的铱坩埚成本以及较长的晶体生长周期也制约了其广泛应用。

Liu 等[13, 30, 35]在不同籽晶诱导下采用 CZ 法制备的 Al_2O_3/YAG 共晶陶瓷宏观形貌随籽晶取向变化无明显差异，均表现为表面光滑有光泽、没有明显

表 1　氧化物共晶陶瓷凝固成形技术

Table 1　Solidification forming technology of oxide eutectic ceramic

Solidification forming technology	Temperature gradient/(K·cm^{-1})	Process parameters	Macroscopic size of ceramic samples	Microstructure scale/μm	Mechanical property
Czochralski method, CZ	~100[20]	Pulling rate≤1.5 mm/h, crystal rotation speed≤10 r/min	> ϕ 30 mm×100 mm[13]	20–35[13]	Al_2O_3/YAG eutectic ceramic hardness 13.08 GPa, fracture toughness 2.71 MPa·m$^{1/2}$, flexural strength 200–300 MPa[20]
Laser floating zone melting, LFZM	~10^4[21]	Pulling rate 2–400 μm/s	> ϕ 3 mm×40 mm[21]	<1[22]	Al_2O_3/GAP eutectic ceramic hardness 16.7 GPa, fracture toughness 4.08 MPa·m$^{1/2}$[21]; Al_2O_3/YAG/ZrO_2 eutectic ceramicflexural strength 2.5 GPa[7]
Laser directed energy deposition, LDED	>10^4[23]	Laser power 150–600 W scanning speed 60–500 mm/min Rotation speed of powder feeding plate 10–20 rpm	ϕ (4–5) mm×410 mm[24]	0.5–1.5[25]	Al_2O_3/GAP/ZrO_2 eutectic ceramic hardness 15.79 GPa, fracture toughness 3.40 MPa·m$^{1/2}$[26]
Laser powder bed fusion, LPBF	>10^4[27]	Laser power 150–300 W scanning speed 100–400 mm/min	~70 mm[28]	<0.2[28]	Al_2O_3/GAP eutectic ceramic hardness 17.1 GPa, fracture toughness 4.5 MPa·m$^{1/2}$[29]

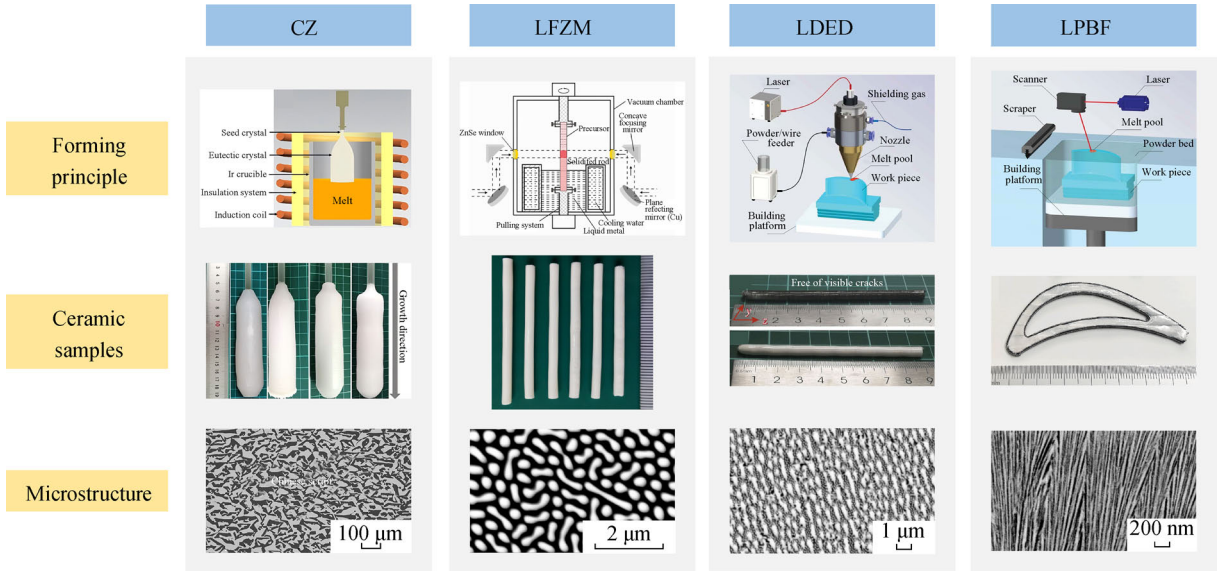


图 1 4 种凝固成形技术的成形原理及其制备的陶瓷样件和微观组织[20–22, 28, 30–34]

Fig. 1 Forming principle of four kinds of solidification forming technology, and the ceramic samples and microstructure prepared by corresponding solidification forming technology[20–22, 28, 30–34]

的裂纹和气孔，颜色呈白色半透明。Al_2O_3/YAG 共晶陶瓷与透明单相籽晶结合良好且稳固。

Hayashi 等[36]研究了氧化物晶体转速对熔体对流和固液界面形状的影响，其界面凸度随晶体转速增大而减小；当晶体转速继续增大，界面形状则会由凸变平、再逐渐凹向熔体。Liu 等[20]进一步将数值模拟与提拉实验相结合，系统探究了提拉速率、晶体转速、晶体直径及保温系统构型对 Al_2O_3/YAG 共晶陶瓷定向凝固过程的影响规律。Liu 等[20]研究表明，通过协同调控生长参数(提拉速率≤1.5 mm/h、晶体转速≤10 r/min、晶体直径≤30 mm)，并采用“25 mm 厚氧化锆保温桶+7 mm 保温棉”的复合保温系统，有效抑制了共晶陶瓷晶体纵切面内显著的沿解理面开裂而形成的宏观裂纹。该系统保证了熔体对流稳定与固液界面微凸的平衡生长状态，实现了大尺寸、无裂纹 Al_2O_3/YAG 共晶陶瓷(ϕ30 mm × 100 mm)的制备，相对密度高达 99.8%。

1.2 LFZM

LFZM 利用高能激光束局部加热并熔化试样，依靠熔体自身重力与表面张力的平衡形成稳定的悬浮熔区，并通过试样与激光束的快速相对抽拉实现平界面定向凝固[21]。该方法的优点在于其极高的温度梯度(~10^4 K/cm)和凝固速率，不仅能有效实现共晶组织的超细化，而且能够在较宽凝固速率范围内对微观组织进行调控。然而，高冷却速率加剧了共晶陶瓷本征脆性及多相间热膨胀系数和弹性模量失配带来的负面影响，导致制备的陶瓷试样尺寸受限。此外，光斑尺寸、熔区表面张力等因素同样制约了 LFZM 技术成形棒状试样的直径。

Zhao 等[7, 37]、Ma 等[22]和 Ren 等[38]采用 LFZM 技术获得了表面光滑、平直无裂纹的高质量 Al_2O_3/YAG、Al_2O_3/YAG/ ZrO_2、Al_2O_3/GAP 和 Al_2O_3/GAP/ZrO_2 等多种体系的氧化物共晶陶瓷，如图 1 所示。通过激光悬浮区熔定向凝固制备共晶复合陶瓷时，需根据稳定熔区的形状来确定形成稳定熔区时特征尺寸的范围。例如，当抽拉速率为 16 μm/s、激光功率为 400 W 时获得了直径为 2.8 mm 的共晶陶瓷试样，其稳定的熔区高度约为 3.5 mm。

基于表面张力梯度与气泡动力学分析，Su 等[31]和 Ren 等[39]揭示了氧化物共晶陶瓷激光快速凝固过程中气泡的分布规律及形成机制。如图 2 所示，在低凝固速率(10 μm/s)下能够稳定获得高致密度无气孔试样；当速率大于 25 μm/s 时，共晶陶瓷试样中心开始出现直径约 300 μm 的孤立气孔；凝固速率进一步提高至 200 μm/s，则导致大量均匀气孔形成，且气孔沿固液界面的法向生长，分布模式由间歇态向连续态转变。固液界面前沿的液相均质形核是气泡的主要形成机制，其生长受扩散与粗化控制[31]；当气泡尺寸达到临界值后，浮力与马兰戈尼力协同驱动气泡脱离界面向熔体迁移。据此建立了气泡形核–长大动力学模型[31, 40]，并通过创新性采用惰性气体保护、高温预热及工艺参数协同优化策略[40, 41]，成

功抑制了快速凝固引发的气孔缺陷，实现了全致密、无裂纹共晶陶瓷的高效可控制备。

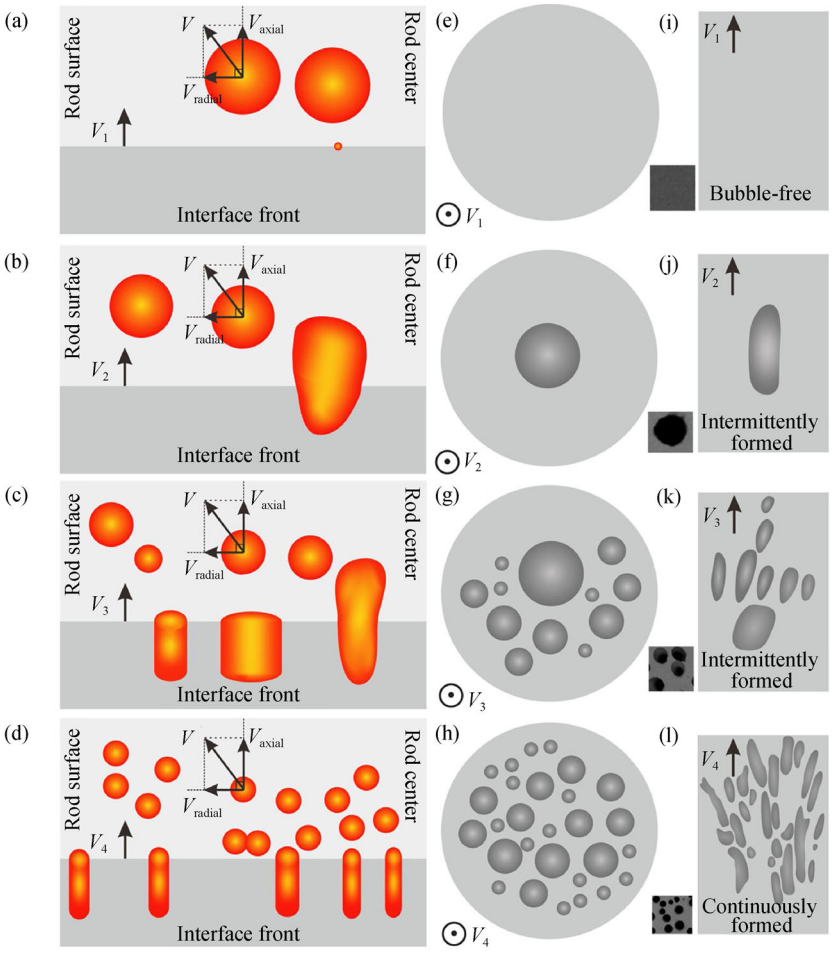


图 2　不同凝固速率下氧化物共晶陶瓷内部气孔的分布特征(V_1<V_2<V_3<V_4)[31]：(a~d)为气孔形成过程示意图；(e~h)为气孔在横截面上的分布特征；(i~l)为气孔在纵截面上的分布特征

Fig. 2　Distribution characteristics of pores in oxide eutectic ceramics at different solidification rates (V_1<V_2<V_3<V_4)[31]: (a–d) is the schematic diagram of stomatal formation process; (e–h) is the distribution characteristics of pores in the cross section; (i–l) is the distribution characteristics of pores in the longitudinal section

1.3　LDED

LDED 基于激光同轴送粉，在惰性气氛中粉末材料被高能激光瞬时熔凝并逐层堆积成形，如图 1 所示。该技术无需黏结剂，能够直接熔凝高熔点氧化物共晶粉末，并获得超细凝固组织；成形效率高，支持复杂结构制造；成形尺寸理论上仅受设备空间限制；搭配多筒送粉器可实现多种材料任意复合与成分梯度设计。但 LDED 技术同样存在粉末利用率偏低、热应力累积导致大尺寸试样易开裂[24]、工艺参数优化难度大、成形精度较低等问题。

随着研究学者对 LDED 成形氧化物陶瓷的不断探索，陶瓷试样的宏观尺寸和成形质量得到提高。Balla 等[42]和 Bernard 等[43]制备了截面尺寸为 8 ~ 25 mm 的圆柱体、齿轮状 Al_2O_3 陶瓷，经热处理后致密度达 98%；Su 等[44]使用 LDED 技术获得了表面光洁、致密度近 100%的棒状和块状 Al_2O_3/YAG 共晶陶瓷；Niu 等[45–48]和 Yang 等[49]通过工艺优化和缺陷控制，制备出具有纳米微观结构的 Al_2O_3、Al_2O_3/ZrO_2 共晶陶瓷壁状和圆柱状试样；Hu 等[50]和 Fan 等[23, 51]同样使用 LDED 技术获得了高致密的块体 Al_2O_3/ZrO_2 和薄壁 Al_2O_3/ YAG/ZrO_2 共晶陶瓷。

经过不断探索，优化工艺参数[52–54]、缩短扫描长度[24]、控制成形舱的氧含量、使用球形粉末作为原料[18]及外场辅助[50, 55]等工艺优化措施均能有效抑制 LDED 制备氧化物陶瓷的裂纹、气孔等凝固缺陷。以此为基础，Su 等[24]和 Liu 等[33, 56]成功实现高致密、大长径比氧化物共晶陶瓷的高效制备。通过精确协同控制扫描长度与扫描速率将单个沉积层加工时间保持为 1.25 s，确保沉积高度随层数线性递增，最终制备出直径 4 mm、高度超 410 mm 的棒状共晶

陶瓷，为目前已报道的陶瓷样件最高沉积高度。Jiang 等[18]使用等离子球化 Al_2O_3 粉末制备的棒状陶瓷弯曲强度达 276.6 MPa，并经工艺优化制备出宽 30 mm 的无裂纹薄壁陶瓷，宽度方向成形误差仅为 5.7%。

1.4 LPBF

LPBF 通过分层切片设置高能激光束选择性熔融粉末薄层，经逐层铺粉–熔凝循环累积成形陶瓷样件[32]。与 LDED 技术类似，LPBF 技术凭借高激光能量密度可实现粉末完全熔融，无需脱脂烧结，缩短制备周期；同时高凝固速率显著细化微观组织。但相较于 LDED 技术，LPBF 技术激光光斑尺寸更小，成形精度高，适用于异形复杂结构制造。

然而极高的温度梯度与冷却速率导致热应力累积，易引发裂纹与翘曲变形，制约大尺寸氧化物陶瓷制备。Shishkovsky 等[57]制备的多孔 Al_2O_3/ZrO_2 陶瓷表面粗糙，内部存在缺陷。Guan 等[58]成形的 10 mm×10 mm×5 mm 立方体出现显著粉末球化。Shen 等[27, 28, 59]利用有限元热力耦合数值模拟与实验结果相互验证并迭代优化，建立了适用于 $Al_2O_3/GAP/ZrO_2$ 共晶陶瓷的 LPBF 成形工艺窗口和扫描策略，实现复杂形状共晶复合陶瓷的高质量成形，包括尺寸约为 30 mm×30 mm×1 mm 的三角形、正方形、正六边形和圆形试样，以及轮廓尺寸约 70 mm 的涡轮叶片薄板状共晶陶瓷，如图 3 所示。



(a) Triangular, square, hexagonal and circular samples (b) Turbine blade sheet with contour size of about 70 mm

图 3 使用 LPBF 技术制备的 $Al_2O_3/GAP/ZrO_2$ 共晶陶瓷样件[27, 28]

Fig. 3 $Al_2O_3/GAP/ZrO_2$ eutectic ceramic samples prepared by LPBF technology[27, 28]

2 凝固组织均细化与晶体取向调控

氧化物共晶陶瓷的凝固过程决定了凝固组织和晶体取向，进而影响陶瓷材料的室温/高温力学、抗氧化、耐腐蚀等性能。尤其是凝固组织的均细化程度和晶体取向显著影响具有高熔化熵和小平面生长特性的氧化物共晶陶瓷材料的强度和高温力学性能。因此，精确控制氧化物共晶陶瓷的凝固组织、调节晶体生长取向，对大尺寸氧化物共晶陶瓷构件的控形控性一体化具有重要的科学意义和工程应用价值。

2.1 凝固组织演变及均细化

凝固制备的 Al_2O_3 基共晶陶瓷凝固组织的形成与演变主要取决于凝固过程的控制，包括固-液界面形态、界面前沿温度梯度和定向凝固速率等。

Ma 等[22, 60–62]系统研究了采用 LFZM 技术制备共晶陶瓷的凝固组织形成及其演变机制。凝固速率为 2 μm/s 时 Al_2O_3/GAP 共晶的固–液界面形貌起伏较大，Al_2O_3 相凸向液相领先生长，与之相邻的 GAP 相中心凹陷[61]。随着凝固速率的增大，固–液界面发生了平–胞转变[3]，凝固速率为 16 μm/s 时形成了共晶胞组织。共晶各相依靠界面附近液相中的溶质横向扩散合作生长，固–液界面为非等温界面。在较宽成分和凝固速率范围内，Al_2O_3/GAP 共晶组织呈现象形文字结构、棒状规则结构和复杂规则结构的多样形貌，如图 4 所示[62]。

随着凝固速率的增大，Al_2O_3/GAP 共晶组织形貌由象形文字结构非规则共晶形貌演变为棒状规则共晶规则共晶形貌。由图 5a~图 5c 可见，凝固速率不高于 16 μm/s 时，Al_2O_3/GAP 共晶呈现均匀分布的象形文字结构非规则共晶形貌，该组织形貌的形成与 Al_2O_3 小平面相和 GAP 非小平面相的本征特性有关。随着凝固速率的增大，Al_2O_3/GAP 共晶的固–液界面由平界面演变为胞状界面，形成了共晶胞组织。如图 5d 所示，凝固速率为 30 μm/s 时，共晶胞内部全为象形文字结构非规则共晶组织。进一步增大凝固速率，如图 5e 和图 5f 所示，共晶胞边缘出现了棒状结构的规则共晶组织，共晶

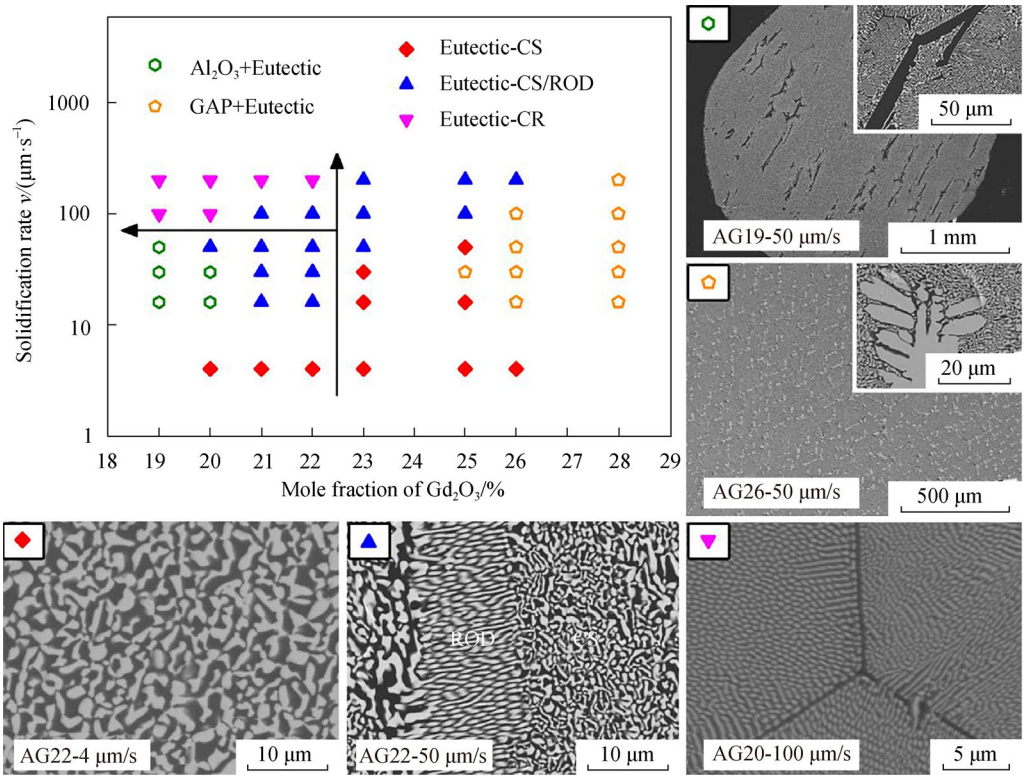


图 4　不同成分和凝固速率下获得的 Al_2O_3/GAP 共晶体系的凝固组织(CS、ROD 和 CR 分别表示象形文字结构、棒状结构和复杂规则结构)[62]

Fig. 4　Solidification microstructures of Al_2O_3/GAP eutectic system with different compositions and solidification rates (CS, ROD and CR represent Chinese script structure, rod structure and complex regular structure, respectively)[62]

胞内部形成了象形文字结构和棒状结构共存的组织形貌，并且棒状结构规则共晶在共晶胞内部的占比逐渐增大。当凝固速率达到 400 μm/s 时，共晶胞内部几乎全部为棒状规则共晶组织，共晶间距仅为(193±20) nm，如图 5g 和图 5f 所示[61]。Zhao 等[63]在 Al_2O_3/YAG/ZrO_2 共晶陶瓷中发现了类似的非规则–规则转变现象。当凝固速率为 300 μm/s 时，Al_2O_3/YAG/ZrO_2 共晶陶瓷横截面内的共晶间距显著细化至(140±17) nm[37]。

使用 LDED 技术制备 Al_2O_3/GAP/ZrO_2 共晶陶瓷时，Liu 等[33]发现在逐层熔覆过程中沉积层顶部发生重熔，超细化凝固组织发生快速粗化，沿沉积方向形成了的周期性带状组织粗大区。通过增大扫描速率以降低熔池的热影响，使带状区的厚度由 48 mm/min 时的 24.8 μm 减小到 192 mm/min 时的 9.2 μm[33]。此外，Liu 等[56]基于组织粗化尺寸效应，发展了适用于激光增材制造共晶陶瓷组织均匀化的高温退火法，在 1500 ℃/300 h 条件下完全消除了凝固组织不均匀性。

2.2　晶体取向调控

采用定向凝固技术制备氧化物共晶陶瓷时，共晶相分别受自身高熔化熵、小平面生长特性，在定向热流驱动下从熔体中析出。氧化物共晶陶瓷的相界面具有特定晶体学取向关系，进而决定了材料的物理和力学等关键性能。籽晶诱导和调控凝固速率是实现共晶陶瓷晶体取向有效调控的重要方法。

Liu 等[13, 30, 35]考察了基于不同籽晶取向诱导条件下，定向凝固共晶陶瓷的竞争生长行为和晶体学取向演变。在单晶籽晶诱导共晶生长纵截面界面连接处，Al_2O_3 相均能继承籽晶晶体学取向，而 YAG 相仅在<111>YAG 籽晶的诱导下能在纵截面处继承籽晶取向，其他情况下均表现为多晶织构[30]。沿定向凝固方向，籽晶外延生长优先控制共晶中同一晶型的晶体学取向。如图 6 所示，当$<11\bar{2}0>Al_2O_3$和$<10\bar{1}0>Al_2O_3$籽晶诱导共晶生长时，沿定向凝固方向共晶中 Al_2O_3 相均能成功稳定继承籽晶取向生长，并且该 2 种取向存在激烈的竞争，偏离度不一。而$<0001>Al_2O_3$籽晶不能调控共晶的晶体学取向，两相仅能通过自调节控制平面错合度在 22%以内。<111>YAG 籽晶会快速筛选 YAG 相的生长取向，但随后 YAG 相择优取向会在最小界面能驱动下在<111>和<101>间变化[13]。

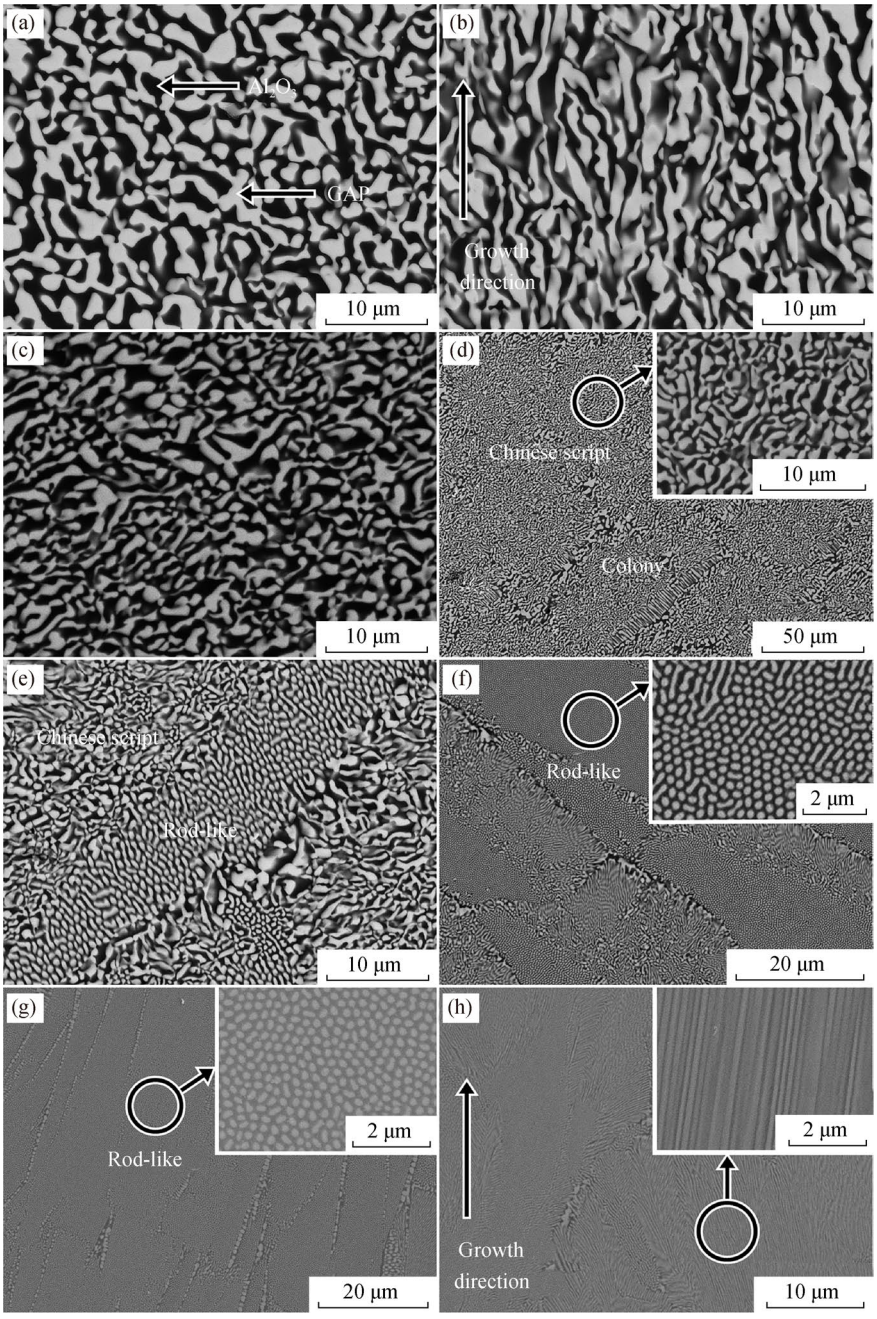


图 5 不同凝固速率下获得的 Al_2O_3/GAP 共晶组织[61]：(a~b) 4 μm/s, (c) 16 μm/s, (d) 30 μm/s, (e) 50 μm/s, (f) 100 μm/s, (g~h) 400 μm/s，其中(b)和(h)为纵截面，其他为横截面

Fig. 5 Microstructures of Al_2O_3/GAP eutectics obtained at different solidification rates[61]: (a–b) 4 μm/s, (c) 16 μm/s, (d) 30 μm/s, (e) 50 μm/s, (f) 100 μm/s, (g–h) 400 μm/s, in which (b) and (h) are longitudinal sections and others are transversal sections

凝固速率对小平面相的组织形貌、择优生长方向等影响显著。Su 等[64]研究了在较宽凝固速率范围下(2~300 μm/s)凝固速率对定向凝固强小平面相的择优生长取向以及平面错合度的影响。随着生长动力学条件的变化，晶体学取向的稳定性随凝固速率的提高逐渐变差，平面错合度由 1.04%(10 μm/s)逐渐增大至 15.84%(100 μm/s)。当凝固速率继续提高至 200 μm/s 时，各个低界面能的晶体学取向关系之间存在强烈的竞争，导致晶体学取向多样化，此时具有高熔化熵、小平面特性的 Al_2O_3/YAG 共晶陶瓷难以实现单晶织构样品的制备。此外，在共晶定向凝固生长过程中，生长动力学因素对晶体学取向的调控作用显著高于界面能。随凝固速率增大，Al_2O_3 相晶体学取向的演变历程为：在 $<10\bar{1}0>$ 和 $<11\bar{2}0>$ 之间徘徊，之后强烈趋于 $<10\bar{1}0>$，最后出现最利于结晶潜热释放的 $<0001>$ 取向。

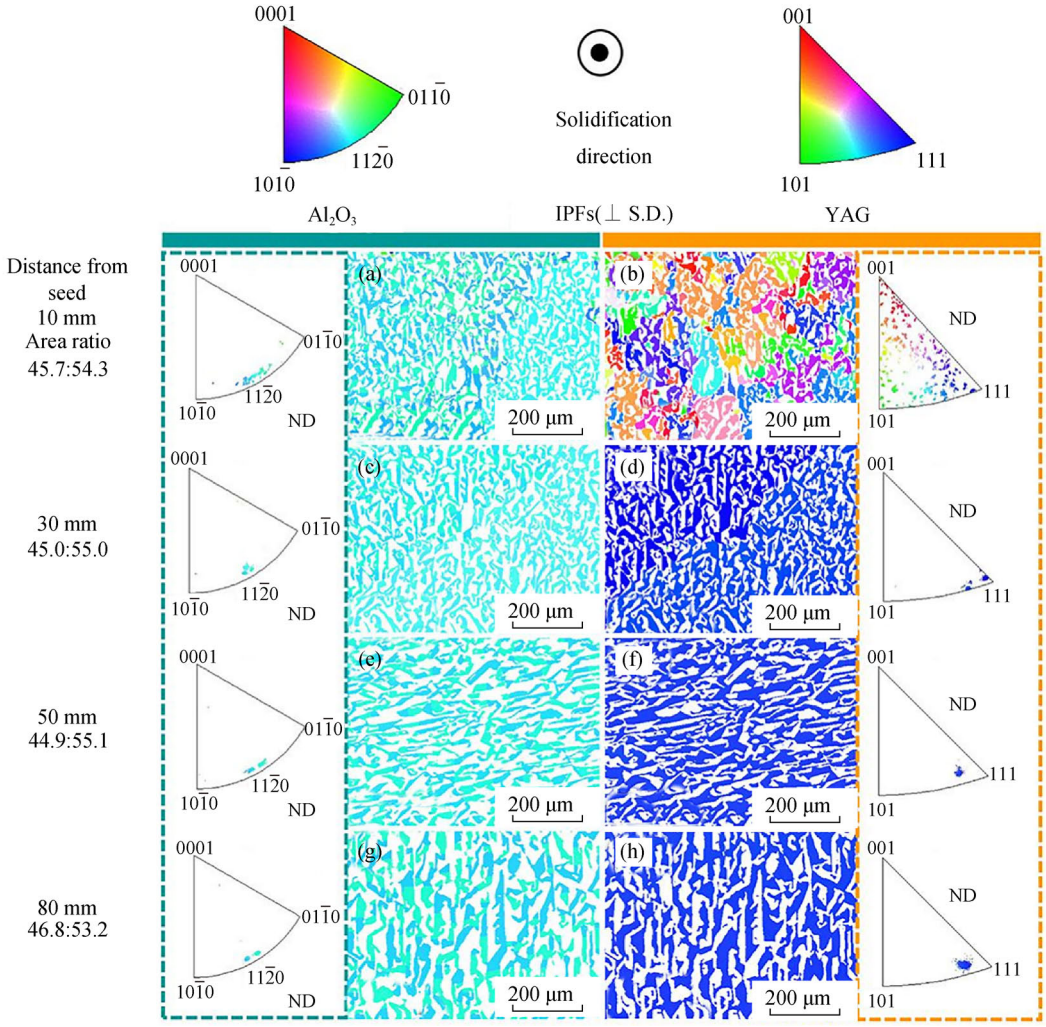


图 6　a 轴 $<11\bar{2}0>$ Al_2O_3 籽晶诱导下距离籽晶不同距离 Al_2O_3/YAG 共晶陶瓷横截面的晶体学取向 EBSD 结果[13]：(a~b) 10 mm; (c~d) 30 mm; (e~f) 50 mm; (g~h) 80 mm；其中，(a)、(c)、(e)、(g)为 Al_2O_3 相的晶体学取向 EBSD 谱，(b)、(d)、(f)、(h)为 YAG 相的晶体学取向 EBSD 谱

Fig. 6　Typical crystallographic orientation EBSD results of Al_2O_3/YAG eutectic ceramic samples at different distances by the a-axis $<11\bar{2}0>$ Al_2O_3 single crystal seed induction[13]: (a–b) 10 mm; (c–d) 30 mm; (e–f) 50 mm; (g–h) 80 mm. Among them, (a), (c), (e), (g) are the crystallographic orientation EBSD maps of Al_2O_3, while (b), (d), (f), (h) are that of YAG

3　力学性能及失效机理

熔体生长氧化物共晶陶瓷因其具有高熔点、优异的力学性能和高温综合性能，被认为是满足高温氧化腐蚀环境中长期服役需求的新型高温结构材料。因此，考察氧化物共晶陶瓷的室温/高温力学性能、高温组织稳定性及耐高温钙镁铝硅酸盐(CaO–MgO–Al_2O_3–SiO_2，CMAS)腐蚀性能等，对该材料的发展和应用具有重要价值。

3.1　室温力学性能

使用 CZ 法制备具有不同晶体学织构的 Al_2O_3/YAG 共晶陶瓷，其硬度和断裂韧性各向异性趋势不明显，硬度和断裂韧性的平均值分别为 13.08 GPa 和 2.71 MPa·$m^{1/2}$[20]，如图 7a 所示，低于 LFZM 制备的同种共晶陶瓷[65]。使用 CZ 法制备的 Al_2O_3/YAG 共晶陶瓷压缩强度变化幅度较大，在 1000 ~ 2000 MPa 浮动，弯曲强度则保持在 200~300 MPa 范围内[20]，如图 7b 所示。

Zhao 等[7]采用 LFZM 制备 Al_2O_3/YAG/ZrO_2 共晶陶瓷时，发现随着凝固速率的提升，弯曲强度呈现出先升高后下降的变化趋势。在凝固速率为 100 μm/s 时，弯曲强度达到最高值 2.5 GPa，是同成分烧结多晶陶瓷的 5 倍。此外，Zhao 等[40]通过调整 LFZM 工艺参数制备了高强度多孔复合陶瓷，在孔隙率为 34%时，室温弯曲强度高达 497 MPa，刷新了目前多孔陶瓷的强度纪录。

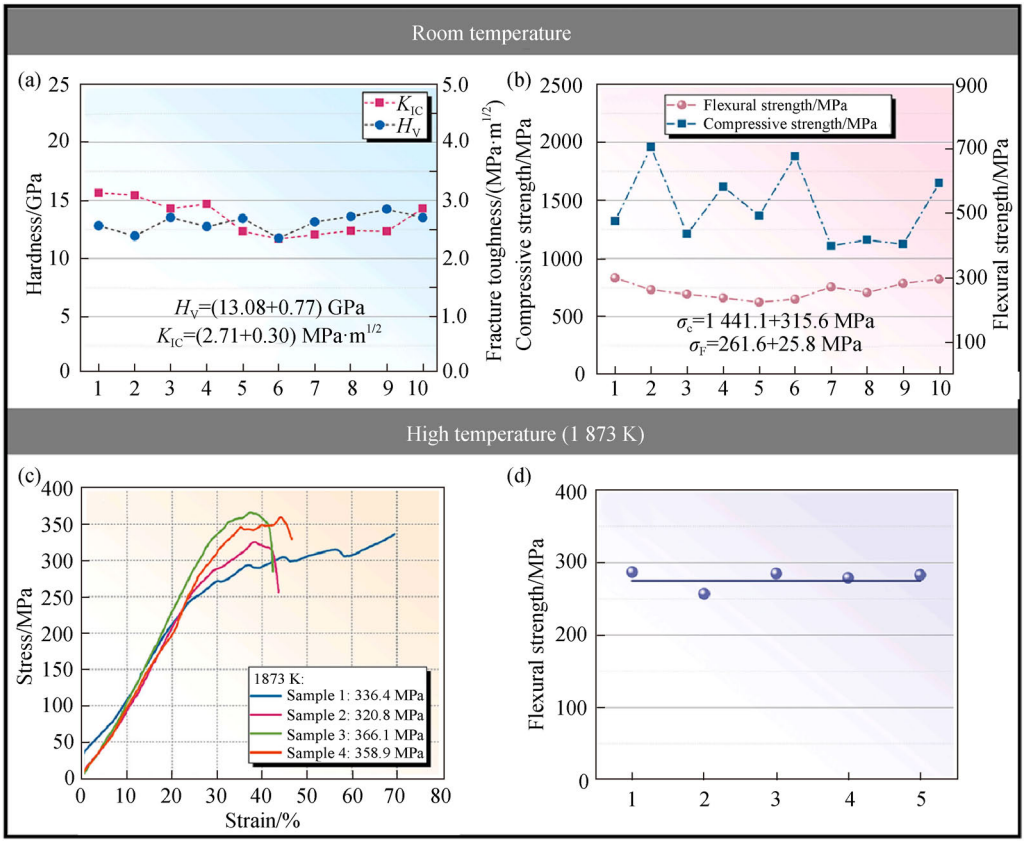


图 7 Al_2O_3/YAG 共晶陶瓷的力学性能[20]：(a)室温硬度和断裂韧性；(b)室温压缩强度和弯曲强度；1873 K 高温下的(c)压缩强度和(d)弯曲强度

Fig. 7 Mechanical properties of Al_2O_3/YAG eutectic ceramic[20]: (a) hardness and fracture toughness at room temperature; (b) compressive strength and flexure strength at room temperature; (c) compressive strength and (d) flexure strength at high temperature of 1873 K

Jiang 等[18]考察了不同形状粉末对 LDED 氧化物共晶陶瓷力学性能的影响。使用等离子球化和非规则 Al_2O_3 粉末 2 种实心粉末分别制备棒状陶瓷并进行力学性能测试。结果表明，非规则粉末制备的 Al_2O_3 陶瓷的显微硬度和断裂韧性更高，分别达到 17.77 GPa 和 4.58 MPa·m$^{1/2}$；而等离子球化 Al_2O_3 粉末制备的棒状试样致密度超 99%，弯曲强度达到 276.6 MPa，如图 8 所示。Shen 等[28]采用 LPBF 制备的 Al_2O_3/GAP/ZrO_2 共晶陶瓷因具备超细共晶组织和强结合界面，最大断裂韧性为 4.76 MPa·m$^{1/2}$，最大硬度达到 18.1 GPa。作为对比，Liu 等[66]使用 LDED 制备的同种共晶陶瓷的硬度和断裂韧性分别为 16.27 GPa 和 3.39 MPa·m$^{1/2}$。

3.2 高温力学性能

Liu 等[20]利用 CZ 法定向凝固获得的不同晶体取向的 Al_2O_3/YAG 共晶陶瓷的高温压缩强度在 320~370 MPa 范围内变化，如图 7c 所示。Al_2O_3/YAG 共晶的弯曲强度保持了良好的高温稳定性，抗弯强度值保持在 270~290 MPa(图 7d)。此外，具有 1500 ℃和 1600 ℃ Al_2O_3/YAG 共晶的三点弯断口形貌表明该高温结构材料的高温弯曲强度对缺陷的敏感性要高于局部非均匀组织；氧化物共晶陶瓷内发生了晶内和穿晶混合形式断裂，是典型的脆性断口形貌[30]。得益于共格/半共格的强结合相界面，Zhao 等[40]制备的多孔氧化物陶瓷在 1500 ℃高温环境下依然具有 324 MPa 的弯曲强度。

3.3 高温组织稳定性及耐腐蚀性能

LDED 制备的 Al_2O_3/GAP/ZrO_2 共晶陶瓷在 1400 ℃高温下热暴露 200 h 后质量不变，亚微米尺度的共晶组织未发生明显粗化，经抛光的试样表面粗糙度几乎无变化[25]。在高于 1400 ℃的高温下长时热暴露后，Al_2O_3/GAP/ZrO_2 共晶陶瓷的微观组织先后出现了非连续粗化、连续粗化及组织合并 3 种粗化方式[25]。

Zhao 等[37]使用 300 μm/s 高凝固速率获得的微纳米 Al_2O_3/YAG/ZrO_2 共晶陶瓷在 1300 ℃热暴露 100 h 后组织未出现明显粗化，表现出优异的高温组织稳定性，说明其取向织构以及半共格低能相界面

依然发挥着重要作用。同样采用 LFZM 技术制备的 Al_2O_3/GAP 和 Al_2O_3/GAP/ZrO_2 共晶试样在 1500 ℃热暴露 500 h 后表现较好的组织稳定性，共晶间距与热暴露时长满足 Ostwald 熟化关系。组织粗化速率随热暴露时长增加而减小，热暴露 500 h 后组织粗化速率小于 0.002 μm/h。

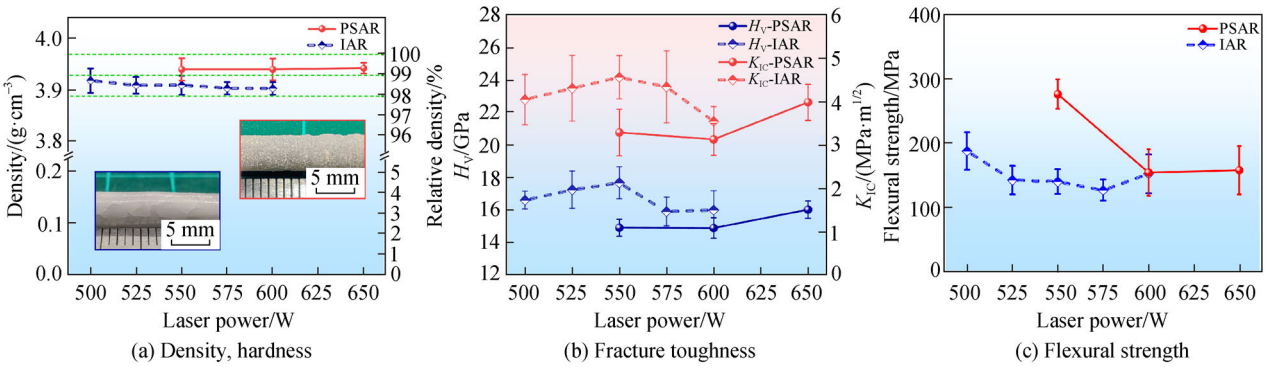


图 8　使用等离子球化和非规则粉末制备的 Al_2O_3 陶瓷物理性能对比[18]

Fig. 8　Comparison of physical properties of Al_2O_3 ceramics prepared by plasma spheroidized and irregular powders[18]

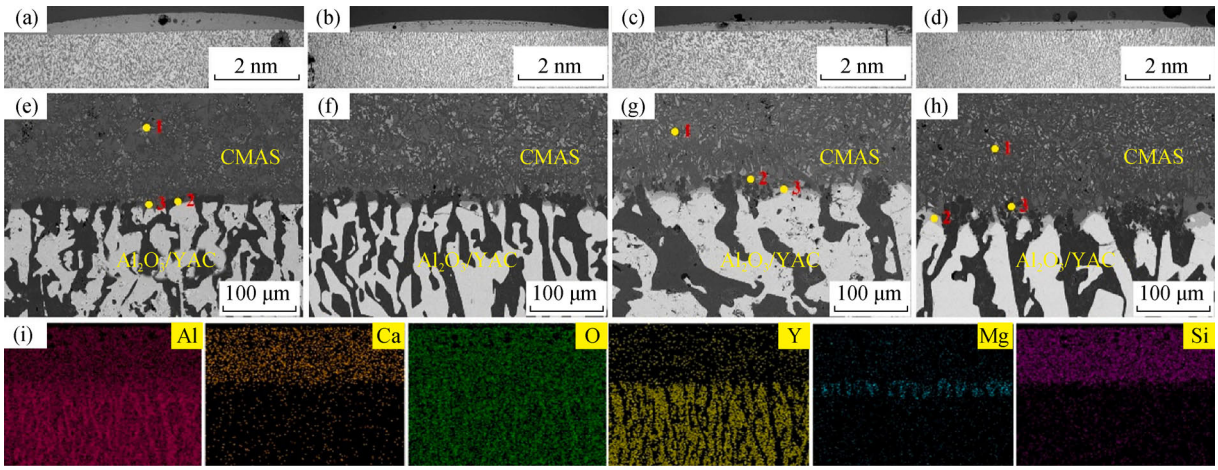


图 9　Al_2O_3/YAG 共晶陶瓷在 1300 ℃下 CMAS 腐蚀后的横截面[10]：(a) 4h、(b) 16h、(c) 50h、(d) 100h 后的腐蚀深度; CMAS 腐蚀(e) 4h、(f) 16h、(g) 50h、(h) 100h 后横截面的 SEM 图像; (i) CMAS 腐蚀 100 h 后横截面的 EDS 图

Fig. 9　Transversal sections Al_2O_3/YAG eutectic ceramic after CMAS corrosion at 1300℃[10]: corrosion depth after (a) 4h, (b) 16h, (c) 50 h, (d) 100h; SEM images of transversal sections after (e) 4h, (f) 16h, (g) 50h, (h) 100h; (i) EDS maps of the transversal section after 100 h

Tan 等[10]研究了采用 CZ 法制备的定向凝固 Al_2O_3/YAG 共晶陶瓷在 1300~1500 ℃的耐高温 CMAS 熔盐腐蚀性能，如图 9 所示。高温下熔融态 CMAS 与氧化物陶瓷组分发生化学反应，生成钙长石($CaAl_2Si_2O_8$)等新相，形成腐蚀层并恶化共晶陶瓷的力学性能。在 1300 ℃腐蚀 100 h 后未观察到腐蚀痕迹。在 1400 ℃和 1500 ℃腐蚀 50 h 后腐蚀深度达到 306 μm 和 316 μm，腐蚀速率没有明显提高。Sun 等[67]使用光学浮区法制备的定向凝固 Al_2O_3/YAG 共晶陶瓷在 1500 ℃腐蚀 100 h 后的凹陷深度约为 130 μm，表明其具有出色的 CMAS 耐腐蚀性。Al_2O_3/YAG 共晶陶瓷表现出良好的耐高温 CMAS 熔盐腐蚀性归因于稳定相界面对 CMAS 渗透的抑制、元素扩散对 CMAS 腐蚀活性的调节及并连续且致密石榴石层的形成[67, 68]。

4　结论与展望

超高温氧化物共晶陶瓷具备杰出的抗氧化、耐腐蚀、组织稳定性和高温力学性能，有望成为高温氧化腐蚀环境中长期服役的新一代高温结构候选材料之一。然而，目前氧化物共晶陶瓷的工程化应用面临大尺寸复杂共晶陶瓷构件成形技术不成熟、凝固缺陷抑制难、韧性低等关键瓶颈难题。因此，需要继续推进氧化物共晶陶瓷大尺寸复杂构件的控形控性一体化研究进程，主要表现在以下 3 个方面：

1) 攻克大尺寸复杂陶瓷构件的高梯度凝固成

形难题：原位揭示高熔点多元复相氧化物共晶在超高温度梯度(~10^4 K·cm^{-1})及非均匀热场下的凝固路径与相选择行为，阐明多相竞争生长与界面失稳的动力学机制，开发热力学调控导向的高效凝固成形技术，为精确控形控性奠定理论基础。

2) 探明大尺寸陶瓷非平衡凝固下的“尺寸效应”并实现缺陷抑制：系统研究构件特征尺寸跃升(从毫米级到分米级)对共晶组织空间分布均匀性(相尺寸、晶体取向、微观组织形貌)及内应力/微裂纹演化的影响规律；探索微区定向凝固调控与外场辅助技术，建立跨尺度凝固组织与缺陷预测模型，实现大体积、大尺寸内微观组织均细化和近无缺陷凝固。

3) 基于界面调控与缺陷抑制的氧化物共晶陶瓷多级协同强韧化：探明氧化物共晶陶瓷在复杂服役工况(高温氧化、水氧/熔盐腐蚀等)下的失效机制，创新陶瓷相界面设计与缺陷抑制策略(如引入可控亚稳态相、设计梯度/复合结构等)，发展原位增韧与外场辅助强化相结合的多级增韧技术，实现氧化物共晶陶瓷的强韧性能的协同提升。

参考文献:

[1] ZHANG X S, CHEN Y J, HU J L. Recent advances in the development of aerospace materials[J]. Prog Aerosp Sci, 2018, 97: 22–34.

[2] BINNER J, PORTER M, BAKER B, et al. Selection, processing, properties and applications of ultra-high temperature ceramic matrix composites, UHTCMCs–a review[J]. Int Mater Rev, 2020, 65(7): 389–444.

[3] SU H J, SHEN Z L, MA W D, et al. Comprehensive microstructure regularization mechanism and microstructure–property stability at 1773 K of directionally solidified Al_2O_3/$GdAlO_3$ eutectic ceramic composite[J]. Compos Part B Eng, 2023, 256: 110647.

[4] SUN L C, ZHOU C, DU T F, et al. Directionally solidified Al_2O_3/$Er_3Al_5O_{12}$ and Al_2O_3/$Yb_3Al_5O_{12}$ eutectic ceramics prepared by optical floating zone melting[J]. J Inorg Mater, 2021, 36(6): 652.

[5] WANG X, ZHANG W, ZHONG Y J, et al. Introduction of low strain energy $GdAlO_3$ grain boundaries into directionally solidified Al_2O_3/$GdAlO_3$ eutectics[J]. Acta Mater, 2021, 221: 117355.

[6] LIU Y, SU H J, LIU H F, et al. Research progress on directionally solidified Al_2O_3/YAG: Ce^{3+} eutectic composite ceramic phosphor for white light emitting diode[J]. J Chin Ceram Soc, 2021, 49(4): 708–722.

[7] ZHAO D, SU H J, LU B H, et al. Ultra-high strength micro-nano quasi-monocrystalline Al_2O_3/$Y_3Al_5O_{12}$/ZrO_2 ternary eutectic ceramics processed by high-speed directional solidification[J]. J Eur Ceram Soc, 2025, 45(13): 117485.

[8] HAO S Q, SU H J, ZHAO D, et al. Complex shaped Al_2O_3/YAG/ZrO_2 eutectic ceramics with excellent high temperature mechanical properties printed by vat photopolymerization[J]. Addit Manuf, 2025, 101: 104703.

[9] WAKU Y, NAKAGAWA N, WAKAMOTO T, et al. A ductile ceramic eutectic composite with high strength at 1, 873 K[J]. Nature, 1997, 389(6646): 49–52.

[10] TAN X, SU H J, LIU Y, et al. CMAS corrosion resistance and mechanism of directionally solidified Al_2O_3/YAG eutectic ceramics at high temperatures of 1300–1500 ℃[J]. Corros Sci, 2025, 248: 112793.

[11] NAKAGAWA N, OHTSUBO H, MITANI A, et al. High temperature strength and thermal stability for melt growth composite[J]. J Eur Ceram Soc, 2005, 25(8): 1251–1257.

[12] WANG X, ZHANG N, ZHONG Y J, et al. Microstructure evolution and crystallography of directionally solidified Al_2O_3/$Y_3Al_5O_{12}$ eutectic ceramics prepared by the modified Bridgman method[J]. J Mater Sci Technol, 2019, 35(9): 1982–1988.

[13] LIU Y, SU H J, SHEN Z L, et al. Effect of seed orientations on crystallographic texture control in faceted Al_2O_3/YAG eutectic ceramic during directional solidification[J]. J Mater Sci Technol, 2023, 146: 86–101.

[14] CARROZ L, DUFFAR T. Tuning the sapphire EFG process to the growth of Al_2O_3/YAG/ZrO_2: Y eutectic[J]. J Cryst Growth, 2018, 489: 5–10.

[15] BENAMARA O, LEBBOU K. Shaped ceramic eutectic plates grown from the melt and their properties[J]. J Cryst Growth, 2016, 449: 67–74.

[16] LIU Y, SU H J, SHEN Z L, et al. Insight into the complex coupled growth behavior of Al_2O_3/YAG eutectic ceramic based on the evolutions of microstructure and crystallographic texture[J]. J Eur Ceram Soc, 2023, 43(10): 4482–4497.

[17] LIU Y, ZHANG M F, WU D, et al. Microstructures and mechanical properties of Al_2O_3/YAG: Ce^{3+} eutectics with different Ce^{3+} concentrations grown by HDS method[J]. J Alloys Compd, 2020, 816: 152515.

[18] JIANG H, SU H J, YU M H, et al. Insights into the influence of powder particle shape on forming process and mechanical properties of Al_2O_3 ceramic fabricated by laser directed energy deposition[J]. Addit Manuf, 2024, 81, 103984.

[19] SHEN Z L, SU H J, YU M H, et al. Synergistic dual-scale laser beams for fabricating high-temperature eutectic ceramic coatings with nano microstructures *via* LPBF[J]. J Mater Sci Technol, 2025, 234: 292–306.

[20] LIU Y, SU H J, TAN X, et al. The effect of processing parameters on the temperature distribution and interface shape in Czochralski growth of Al_2O_3/YAG eutectic ceramic composite: Modeling and experiment[J]. Ceram Int, 2025, 51(22): 36401–36414.

[21] SU H J, REN Q, ZHANG J, et al. Microstructures and mechanical properties of directionally solidified Al_2O_3/$GdAlO_3$ eutectic ceramic by laser floating zone melting with high temperature gradient[J]. J Eur Ceram Soc, 2017, 37(4): 1617–1626.

[22] MA W D, ZHANG J, SU H J, et al. Microstructure transformation from irregular eutectic to complex regular eutectic in directionally solidified Al_2O_3/$GdAlO_3$/ZrO_2 ceramics by laser floating zone melting[J]. J Eur Ceram Soc, 2016, 36(6): 1447–1454.

[23] FAN Z Q, ZHAO Y T, TAN Q Y, et al. Nanostructured Al_2O_3-YAG-ZrO_2 ternary eutectic components prepared by laser engineered net shaping[J]. Acta Mater, 2019, 170: 24–37.

[24] SU H J, LIU H F, JIANG H, et al. One-step preparation of melt-grown Al_2O_3/$GdAlO_3$/ZrO_2 eutectic ceramics with large size and irregular shape by directed energy deposition[J]. Addit Manuf, 2023, 70: 103563.

[25] LIU H F, SU H J, SHEN Z L, et al. Insights into high thermal stability of laser additively manufactured Al_2O_3/$GdAlO_3$/ZrO_2 eutectic ceramics

under high temperatures[J]. Addit Manuf, 2021, 48: 102425.

[26] LIU H F, SU H J, SHEN Z L, et al. Formation mechanism and roles of oxygen vacancies in melt-grown $Al_2O_3/GdAlO_3/ZrO_2$ eutectic ceramic by laser 3D printing[J]. J Adv Ceram, 2022, 11(11): 1751–1763.

[27] SHEN Z L, SU H J, YU M H, et al. Large-size complex-structure ternary eutectic ceramic fabricated using laser powder bed fusion assisted with finite element analysis[J]. Addit Manuf, 2023, 72: 103627.

[28] SHEN Z L, SU H J, YU M H, et al. Unveiling exotic multi-scale microstructure transformation and crack formation mechanisms in eutectic ceramic composite by laser powder bed fusion[J]. Compos Part B Eng, 2025, 288: 111883.

[29] SHEN Z L, SU H J, LIU H F, et al. Directly fabricated $Al_2O_3/GdAlO_3$ eutectic ceramic with large smooth surface by selective laser melting: Rapid solidification behavior and thermal field simulation[J]. J Eur Ceram Soc, 2022, 42(3): 1088–1101.

[30] LIU Y, SU H J, TAN X, et al. Stability of crystallographic texture and mechanical anisotropy toward Al_2O_3/YAG eutectic ceramic composite using single crystalline seeds[J]. Compos Part B Eng, 2024, 274: 111263.

[31] SU H J, LIU Y, REN Q, et al. Distribution control and formation mechanism of gas inclusions in directionally solidified Al_2O_3-$Er_3Al_5O_{12}$-ZrO_2 ternary eutectic ceramic by laser floating zone melting[J]. J Mater Sci Technol, 2021, 66: 21–27.

[32] GU D D, SHI X Y, POPRAWE R, et al. Material-structure-performance integrated laser-metal additive manufacturing[J]. Science, 2021, 372(6545): eabg1487.

[33] LIU H F, SU H J, SHEN Z L, et al. One-step additive manufacturing and microstructure evolution of melt-grown $Al_2O_3/GdAlO_3/ZrO_2$ eutectic ceramics by laser directed energy deposition[J]. J Eur Ceram Soc, 2021, 41(6): 3547–3558.

[34] LIU H F, SU H J, SHEN Z L, et al. Direct formation of $Al_2O_3/GdAlO_3/ZrO_2$ ternary eutectic ceramics by selective laser melting: Microstructure evolutions[J]. J Eur Ceram Soc, 2018, 38(15): 5144–5152.

[35] LIU Y, SU H J, TAN X, et al. Unveiling crystallographic texture in laser floating zone melted Al_2O_3/YAG eutectic ceramic by seed-crystal inducing[J]. Ceram Int, 2024, 50(20): 40185–40190.

[36] HAYASHI A, KOBAYASHI M, JING C J, et al. Numerical simulation of the Czochralski growth process of oxide crystals with a relatively thin optical thickness[J]. Int J Heat Mass Transf, 2004, 47(25): 5501–5509.

[37] ZHAO D, SU H J, HAO S Q, et al. Excellent thermal stability of nanostructured Al_2O_3–$Y_3Al_5O_{12}$–ZrO_2 eutectic ceramic composites by high-speed directional solidification[J]. Compos Part B Eng, 2023, 266: 111035.

[38] REN Q, SU H J, ZHANG J, et al. Effect of an abrupt change in pulling rate on microstructures of directionally solidified Al_2O_3-$Er_3Al_5O_{12}$ eutectic and off-eutectic composite ceramics[J]. Ceram Int, 2019, 45(6): 6632–6638.

[39] REN Q, SU H J, ZHANG J, et al. Processing, microstructure and performance of $Al_2O_3/Er_3Al_5O_{12}/ZrO_2$ ternary eutectic ceramics prepared by laser floating zone melting with ultra-high temperature gradient[J]. Ceram Int, 2018, 44(5): 4766–4776.

[40] ZHAO D, SU H J, LIU Y, et al. Ultrahigh-strength porous ceramic composites *via* a simple directional solidification process[J]. Nano Lett, 2022, 22(6): 2405–2411.

[41] ZHAO D, SU H J, LIU H F, et al. Densification and microstructural evolution of bulk Al_2O_3–$Y_3Al_5O_{12}$(YAG) eutectic ceramic fabricated by spark plasma sintering[J]. Ceram Int, 2019, 45(9): 12337–12343.

[42] BALLA V K, BOSE S, BANDYOPADHYAY A. Processing of bulk alumina ceramics using laser engineered net shaping[J]. Int J Appl Ceram Technol, 2008, 5(3): 234–242.

[43] BERNARD S A, BALLA V K, BOSE S, et al. Direct laser processing of bulk lead zirconate titanate ceramics[J]. Mater Sci Eng B, 2010, 172(1): 85–88.

[44] SU H J, ZHANG J, LIU L, et al. Rapid growth and formation mechanism of ultrafine structural oxide eutectic ceramics by laser direct forming[J]. Appl Phys Lett, 2011, 99(22): 221913.

[45] NIU F Y, WU D J, ZHOU S Y, et al. Power prediction for laser engineered net shaping of Al_2O_3 ceramic parts[J]. J Eur Ceram Soc, 2014, 34(15): 3811–3817.

[46] NIU F Y, WU D J, MA G Y, et al. Nanosized microstructure of Al_2O_3–ZrO_2 (Y_2O_3) eutectics fabricated by laser engineered net shaping[J]. Scr Mater, 2015, 95: 39–41.

[47] NIU F Y, WU D J, MA G Y, et al. Effect of second-phase doping on laser deposited Al_2O_3 ceramics[J]. Rapid Prototyp J, 2015, 21(2): 201–206.

[48] NIU F Y, WU D J, LU F, et al. Microstructure and macro properties of Al_2O_3 ceramics prepared by laser engineered net shaping[J]. Ceram Int, 2018, 44(12): 14303–14310.

[49] YAN S, WU D J, MA G Y, et al. Nano-sized Al_2O_3-ZrO_2 eutectic ceramic structures prepared by ultrasonic-assisted laser engineered net shaping[J]. Mater Lett, 2018, 212: 8–11.

[50] HU Y B, NING F D, CONG W L, et al. Ultrasonic vibration-assisted laser engineering net shaping of ZrO_2-Al_2O_3 bulk parts: Effects on crack suppression, microstructure, and mechanical properties[J]. Ceram Int, 2018, 44(3): 2752–2760.

[51] FAN Z Q, ZHAO Y T, TAN Q Y, et al. New insights into the growth mechanism of 3D-printed Al_2O_3–$Y_3Al_5O_{12}$ binary eutectic composites[J]. Scr Mater, 2020, 178: 274–280.

[52] NIU F Y, WU D J, YAN S, et al. Process optimization for suppressing cracks in laser engineered net shaping of Al_2O_3 ceramics[J]. JOM, 2017, 69(3): 557–562.

[53] SHEN Z L, SU H J, LIU Y, et al. Laser additive manufacturing of melt-grown $Al_2O_3/GdAlO_3$ eutectic ceramic composite: Powder designs and crack analysis with thermo-mechanical simulation[J]. J Eur Ceram Soc, 2022, 42(14): 6583–6598.

[54] SHEN Z L, SU H J, JIANG H, et al. Predicting rapid growth behavior in solidified eutectic ceramic composites using infrared thermal imaging and thermal field simulation during laser directed energy deposition[J]. Compos Part B Eng, 2024, 283: 111619.

[55] YAN S, WU D J, NIU F Y, et al. Effect of ultrasonic power on forming quality of nano-sized Al_2O_3-ZrO_2 eutectic ceramic *via* laser engineered net shaping (LENS)[J]. Ceram Int, 2018, 44(1): 1120–1126.

[56] LIU H F, SU H J, SHEN Z L, et al. Preparation of large-size $Al_2O_3/GdAlO_3/ZrO_2$ ternary eutectic ceramic rod by laser directed energy deposition and its microstructure homogenization mechanism[J]. J Mater Sci Technol, 2021, 85: 218–223.

[57] SHISHKOVSKY I, YADROITSEV I, BERTRAND P, et al. Alumina–zirconium ceramics synthesis by selective laser sintering/melting[J]. Appl Surf Sci, 2007, 254(4): 966–970.

[58] GUAN J R, WANG Q P, ZHANG X W, et al. Selective laser melting of yttria-stabilized zirconia[J]. Mater Res Express, 2019, 6(1): 015402.

[59] SHEN Z L, SU H J, YU M H, et al. Enhanced 3D printing and crack

control in melt-grown eutectic ceramic composites with high-entropy alloy doping[J]. J Mater Sci Technol, 2025, 209: 64–78.

[60] MA W D, SU H J, ZHANG J, et al. Effects of composition and solidification rate on growth striations in laser floating zone melted Al_2O_3/$GdAlO_3$ eutectic ceramics[J]. J Am Ceram Soc, 2018, 101(8): 3337–3346.

[61] MA W D, ZHANG J, SU H J, et al. Theoretical prediction and experimental comparison for eutectic growth of Al_2O_3/$GdAlO_3$ faceted eutectics[J]. J Eur Ceram Soc, 2019, 39(13): 3837–3842.

[62] MA W D, ZHANG J, SU H J, et al. Phase growth patterns for Al_2O_3/$GdAlO_3$ eutectics over wide ranges of compositions and solidification rates[J]. J Mater Sci Technol, 2021, 65: 89–98.

[63] ZHAO D, SU H J, HAO S Q, et al. Insight into faceted-nonfaceted transition of directionally solidified eutectic ceramic composites by laser floating zone melting and infrared imaging[J]. Compos Part B Eng, 2024, 277: 111372.

[64] SU H J, LIU Y, REN Q, et al. Unveiling the dynamic instability mechanism of microstructure transformation in faceted oxide eutectic composite ceramics[J]. J Mater Sci Technol, 2023, 144: 224–234.

[65] WANG X, ZHONG Y J, HU Q D. A review of Al_2O_3-based eutectic ceramics for high-temperature structural materials[J]. J Mater Sci Technol, 2025, 214: 214–232.

[66] LIU H F, JIANG H, SHEN Z L, et al. Microstructure evolution and mechanical property of melt-grown Al_2O_3/$GdAlO_3$/ZrO_2 eutectic ceramics prepared by laser directed energy deposition[J]. Ceram Int, 2024, 50(13): 22565–22573.

[67] SUN H F, SUN L C, REN X M, et al. Outstanding molten calcium–magnesium–aluminosilicate (CMAS) corrosion resistance of directionally solidified Al_2O_3/$Y_3Al_5O_{12}$ eutectic ceramic at 1500 ℃[J]. Corros Sci, 2023, 220: 111289.

[68] LIU Y, SU H J, SHEN Z L, et al. High temperature calcium-magnesium-alumina-silicate (CMAS) corrosion behavior of directionally solidified Al_2O_3/YAG eutectic ceramic[J]. J Mater Sci Technol, 2023, 165: 66–74.

Research Progress on Microstructure Evolution and Mechanical Properties of Ultra-High Temperature Oxide Eutectic Ceramics Solidified by High Temperature Gradient Solidification

JIANG Hao, *SU Haijun*, *YU Minghui*, *WANG Ruotong*, *SHEN Zhonglin*, *GUO Yinuo*, *ZHANG Zhuo*, *GUO Min*
(State Key Laboratory of Solidification Processing, Northwestern Polytechnical University, Xi'an 710072, China)

Extended Abstract

The research and development of ultrahigh-temperature structural materials and advanced preparation technologies that can work stably in extreme environments at >1600 ℃ for a long time is a fundamental guarantee for improving the thrust weight ratio, prolonging the service life and enhancing the reliability of aircraft engines, and become a strategic focus of international competition. At high melting points, high strength, and excellent oxidation and corrosion resistance, ultra-high temperature oxide ceramics are regarded as one of the most promising high-temperature structural materials in high-temperature oxidation environments. However, the microstructure of oxide ceramics prepared by conventional powder sintering technology shows typical polycrystalline structure characteristics. Structural defects (*i.e.*, grain boundary glass phases and weak bonding interfaces) seriously weaken the high-temperature strength, structural stability, and creep resistance of oxide ceramics, making it difficult to fully demonstrate the superior oxidation resistance and corrosion resistance of oxide ceramics in high-temperature and oxygen-enriched environments. In recent years, alumina-based eutectic ceramics prepared by directional solidification technology, based on the principle of liquid-solid transformation, have shown a breakthrough in the field of advanced structural materials. This technology diverges from the conventional ceramic sintering concept and achieves a creative combination of melt growth technology and the exceptional properties of oxide ceramics. However, the solidification characteristics of oxide eutectic ceramics under high-temperature gradients are not well understood, and the forming technology for large-size components is not yet mature. The poor thermal conductivity and high melt viscosity of oxides make it easy to produce solidification defects, such as cracks, pores, and segregation, during the solidification process. The eutectic phases of oxide grown in small planes show an intense anisotropy in microstructure and properties, but they cannot achieve precise control of crystal orientation. The poor toughness of oxide eutectic ceramics also limits their application process.

In this review, the principle and development status of four solidification forming technologies, including the Czochralski method, laser suspension zone melting, laser directional energy deposition, and laser powder bed melting, are summarized, and the formation mechanism and control strategy of defects in the solidification process are also represented. This review focuses on the solidification structure evolution and homogenization method of oxide eutectic ceramics, as well as the influencing factors and control mechanism of crystal orientation selection, as well as the research progress of room- temperature/high-temperature mechanical properties and failure mechanism, high-temperature microstructure stability and high-temperature CMAS corrosion properties of oxide ceramics. Finally, the development trend of high-temperature oxide eutectic ceramics in three aspects of high gradient solidification forming, non-equilibrium solidification defect suppression and multi-level synergistic strengthening and toughening is prospected.

A high-gradient directional solidification and complex component laser additive manufacturing technology for ultra-high

temperature alumina-based eutectic ceramics is established. The mechanisms of defect formation during the solidification process is revealed. This research enables the efficient fabrication of high-density, large-sized, and ultra-fine eutectic ceramic samples, as well as complex components. The non-equilibrium rapid solidification microstructural characteristics and evolution mechanisms of multi-phase oxide eutectic ceramics are revealed. The eutectic-dendrite transition rate and the range of the eutectic coexistence zone are obtained. The crystal orientation selection and competitive growth patterns induced by seed crystals in eutectic ceramics are elucidated. A stable coupled growth model for the faceted eutectic ceramics is established. The evolution mechanisms of high-temperature performance of eutectic ceramics under extreme oxidative corrosion conditions are elucidated. The fabricated porous eutectic ceramics (porosity of 34%) achieve a high bending strength that is an international record (*i.e.*, 497 MPa at room temperature; 324 MPa at 1500 ℃). The high-density eutectic ceramics exhibit a bending strength of up to 2500 MPa at room temperature. After 500-h thermal exposure at 1500 ℃, the microstructural coarsening rate is ≤0.002 μm/h, and the corrosion depth from molten oxide exposure at 1500 ℃ for 100 h is ≤130 μm, demonstrating a superior high-temperature mechanical and environmental performance.

Summary and Prospects Ultra-high temperature oxide eutectic ceramics have superior oxidation resistance, corrosion resistance, microstructure stability, and high-temperature mechanical properties. They are expected to be one of the new high-temperature structural candidate materials, serving for an extended period in high-temperature oxidation-corrosion environments. However, the engineering application of oxide eutectic ceramics faces key bottleneck problems, including the immature forming technology for large-size, complex eutectic ceramic components, the difficulty in inhibiting solidification defects, and low toughness. It is thus necessary to continue to promote the research process of the integration of shape control and property control of large-scale complex components of oxide eutectic ceramics, mainly in the following three aspects, *i.e.*, 1) It is urgent to develop efficient solidification forming technology for large-scale complex ceramic components, and explore the solidification characteristics of high melting point multi-phase oxide eutectic ceramics under high temperature gradient; 2) The effects of process parameters and component size on eutectic structure and solidification defects under non-equilibrium solidification conditions should be explored, and the methods of microstructure refinement and solidification structure inhibition should be established; and 3) It is necessary to clarify the failure mechanism of oxide eutectic ceramics and develop a multi-scale strengthening and toughening technology suitable for high melting point ceramic materials to achieve a synergistic improvement of the strength and toughness of eutectic ceramics.

Keywords oxide eutectic ceramics; solidification forming; microstructure evolution; performance regulation